

On Gas-Drag Induced Rapid Migration of Solids in a Non-Uniform Solar Nebula

Nader Haghighipour and Alan P. Boss

*Department of Terrestrial Magnetism, Carnegie Institution of Washington,
5241 Broad Branch Road, Washington, DC 20015*

nader@dtm.ciw.edu, boss@dtm.ciw.edu

ABSTRACT

We study the motions of small solids, ranging from micron-sized dust grains to meter-sized objects, in the vicinity of local pressure enhancements of a gaseous nebula. Integrating numerically, we show that as a result of the combined effect of gas drag and pressure gradients, solids tend to accumulate at the locations where the pressure of the gas maximizes. The rate of migration of solids varies with their sizes and densities and also with the physical properties of the gas. The results of our numerical simulations indicate that such migrations are most rapid for meter-sized objects. The applicability of the results to the enhancement of the collision and coagulation of solids and also to the growth-rate of planetesimals is discussed.

Subject headings: solar system: formation, planetary systems: formation, planetary systems: protoplanetary disks

1. Introduction

We have recently shown that in a rotating, turbulence-free and isothermal gaseous nebula with a density function that maximizes locally, the combined effect of gas drag and pressure gradients at hydrostatic equilibrium, causes solids to migrate toward the locations of local density enhancements (Haghighipour & Boss 2003, hereafter HB03). The motions of solids in HB03 were restricted to the midplane of the nebula and the variation of the gas density along the direction perpendicular to the midplane was neglected. The results of our numerical simulations of the dynamics of micron-sized dust grains to 100 meter-sized objects indicated that the radial motions of such solids could be quite rapid when their sizes range from 1 cm to 1 m.

In this paper, we extend our previous analysis to three-dimensional motions and study the radial and vertical migrations of solids subject to gas drag and the gravitational attraction of a solar type star in a non-uniform gaseous nebula.

Study of the motions of solids in gaseous mediums has long been of particular interest to astronomers. Because of the great diversity in the applicability of the results of such studies, in particular, to the process of formation of planetesimals, the literature in this area has become so rich that it makes it virtually impossible to cite all the related articles here. For a short review of the history of such studies we refer the reader to HB03 and the references therein. Of direct relevance to this study, however, are two classic papers by Adachi et al. (1976) and Weidenschilling (1977), an article by Supulver and Lin (2000) on the study of the orbital evolution of solids in a turbulent protostellar disk with application to the formation of icy planetesimals in the outer region of the nebula and a recent paper by Takeuchi and Lin (2002) on the radial migration of dust grains in an accreting solar nebula.

Our model nebula is turbulence-free and isothermal. We assume that it consists of pure molecular hydrogen and follows the equation of state of an ideal gas. An enhancement in the pressure of the gas in such a nebula appears where the density of the gas is locally enhanced. To focus attention on the rate of migration of solids and its dependence on their sizes and physical properties, the density of the nebula is assumed to have an azimuthally symmetric maximum on the midplane. Along the vertical axis, the gas density changes in a way that the vertical component of the pressure gradients balances the vertical component of the gravitational force of the central star. The direction of radial motions of solids in our model nebula depends on their initial positions relative to the location of the maximum gas density and their vertical migration is always toward the midplane. (Whipple 1964; Haghighipour & Boss 2003).

We start by explaining our physical model in § 2 and present the equations of motions of solids in § 3. In § 4, we present the results of our numerical simulations and in § 5, we conclude our study by reviewing the results and discussing their applications.

2. The Physical Model

We consider a rotating, turbulence-free, and isothermal gaseous nebula of pure molecular hydrogen with a Sun-like star at its center. At hydrostatic equilibrium and in a cylindrical coordinate system with the star at its origin and the midplane of the nebula as its polar plane, the gravitational attraction of the star at a point with a position vector $\mathbf{R}(r, z)$ is

related to the pressure gradients of the gas as

$$r\omega_g^2 = r\omega_K^2 + \frac{1}{\rho_g(\mathbf{R})} \frac{\partial \mathcal{P}_g(\mathbf{R})}{\partial r} \quad (1)$$

in r -direction and

$$z\omega_K^2 + \frac{1}{\rho_g(\mathbf{R})} \frac{\partial \mathcal{P}_g(\mathbf{R})}{\partial z} = 0 \quad (2)$$

along the z -axis. In equations (1) and (2), $\rho_g(\mathbf{R})$ and $\mathcal{P}_g(\mathbf{R})$ are the density and pressure of the gas, respectively, ω_g is the angular velocity of the gas on a plane parallel to the midplane at a height z , and ω_K is its corresponding Keplerian angular velocity given by

$$\omega_K^2 = \frac{GM}{(r^2 + z^2)^{3/2}}, \quad (3)$$

where G is the gravitational constant and M is the mass of the central star.

The balance of the gravitational attraction of the central star by the pressure gradients in the vertical direction, as given by equation (2), determines the distribution of the gas along the z -axis. In the model nebula considered here, the gas is pure molecular hydrogen and it, therefore, obeys the equation state of an ideal gas. As a result, the pressure and density of the gas are related as

$$\mathcal{P}_g = \frac{K_B T}{m_0} \rho_g(\mathbf{R}), \quad (4)$$

where K_B is the Boltzmann constant, T is the temperature of the gas and m_0 is the molecular mass of hydrogen. Substituting for $\mathcal{P}_g(\mathbf{R})$ from equation (4) in equation (2), the density of our model nebula will be given by

$$\rho_g(r, z) = \rho_g(r, 0) \text{Exp} \left\{ \frac{GMm_0}{K_B T} \left[\frac{1}{(r^2 + z^2)^{1/2}} - \frac{1}{r} \right] \right\}. \quad (5)$$

In equation (5), $\rho_g(r, 0)$ is the density of the gas on the midplane.

As mentioned in § 1, in order to focus attention on the dynamics of solids, we consider a nebula with an azimuthally symmetric density enhancement on its midplane. Following HB03, we assume

$$\rho_g(r, 0) = \rho_0 \text{Exp} \left[-\beta \left(\frac{r}{r_m} - 1 \right)^2 \right], \quad (6)$$

where ρ_0 , r_m and β are constant quantities. Figure 1 shows an edge-on view of our model nebula with the line of sight perpendicular to one of the midplane diameters. The central star in this figure is solar-type and the gas temperature is 300 K. The values of ρ_0 , β and r_m are equal to $10^{-9} \text{ g cm}^{-3}$, 1 and 1 AU, respectively.

3. Equation of Motion

The equation of motion of an object with mass of unity in our model nebula is given by

$$\frac{d^2 \mathbf{R}}{dt^2} = - \frac{GM}{(r^2 + z^2)^{3/2}} \mathbf{R} - \mathbf{F}_{\text{drag}} \quad (7)$$

where \mathbf{F}_{drag} represents the drag force of the gas for the unit mass of a solid. Following Supulver and Lin (2000) and as presented in HB03, we write \mathbf{F}_{drag} as

$$\mathbf{F}_{\text{drag}} = \frac{\rho_g(\mathbf{R})}{\rho_p(a_p + \lambda)} \left[\left(\frac{\lambda}{a_p} \right) \bar{v}_{\text{th}} + \frac{3}{8} C_D v_{\text{rel}} \right] \mathbf{V}_{\text{rel}}. \quad (8)$$

In equation (8), a_p is the radius of the object, ρ_p denotes its density, $v_{\text{rel}} = |\mathbf{V}_{\text{rel}}|$ is the magnitude of its velocity relative to the gas and λ is the mean free path of the gas molecules. For a nebula of pure molecular hydrogen, $\lambda(\text{cm}) = 4.79 \times 10^{-9} / \rho_g(\mathbf{R}) \text{ g cm}^{-3}$ (HB03). The quantity $\bar{v}_{\text{th}} = (8K_{\text{B}}T/\pi m_0)^{1/2}$ in equation (8) is the mean thermal velocity of the gas molecules and C_D is the drag coefficient whose numerical value is given by (Whipple 1964; Weidenschilling 1977)

$$C_D \simeq \begin{cases} 24 \text{Re}^{-1} & \text{if } \text{Re} < 1 \text{ (Stokes' drag)} \\ 24 \text{Re}^{-0.6} & \text{if } 1 < \text{Re} < 800 \\ 0.44 & \text{if } \text{Re} > 800. \end{cases} \quad (9)$$

In equation (9), Re is the gas Reynolds number and is equal to

$$\text{Re} = \left(\frac{6\sigma a_p}{m_0 \bar{v}_{\text{th}}} \right) \rho_g(\mathbf{R}) v_{\text{rel}}, \quad (10)$$

where $\sigma = 2 \times 10^{-15} \text{ cm}^2$ is the collisional cross section of hydrogen molecules.

The velocity of a solid relative to the gas is equal to $\mathbf{V}_{\text{rel}} = \mathbf{V}_p - \mathbf{V}_g$ where \mathbf{V}_p and \mathbf{V}_g represent the velocities of the solid and gas molecules, respectively. In the cylindrical coordinate system considered here, \mathbf{V}_{rel} has the following components.

$$(\mathbf{V}_{\text{rel}})_r = \dot{r}, \quad (11)$$

$$(\mathbf{V}_{\text{rel}})_z = \dot{z}, \quad (12)$$

$$(\mathbf{V}_{\text{rel}})_\varphi = r(\dot{\varphi} - \omega_g). \quad (13)$$

where we have assumed that the gas molecules do not move along the z -axis. It is important to mention that it is the r and z components of \mathbf{V}_{rel} that play important roles in the radial

and vertical migrations of solids. They also dominate the magnitude of \mathbf{V}_{rel} when the object is small. The transverse component of the relative velocity, $(\mathbf{V}_{\text{rel}})_\varphi$, will have a dominating effect in the magnitude of \mathbf{V}_{rel} for larger objects and it plays an important role in changing the angular momenta of such solids which can have significant contributions when accretion is considered.

From equations (11) to (13), the equation of motion of a solid with a unit mass can be written as

$$\hat{P}_r = \dot{\hat{r}}, \quad (14)$$

$$\hat{P}_z = \dot{\hat{z}}, \quad (15)$$

$$\hat{P}_\varphi = \hat{r}^2 \dot{\hat{\varphi}}, \quad (16)$$

$$\dot{\hat{P}}_r = \frac{1}{\hat{r}^3} \hat{P}_\varphi^2 - \frac{\hat{r}}{(\hat{r}^2 + \hat{z}^2)^{3/2}} - (\hat{F}_{\text{drag}})_r, \quad (17)$$

$$\dot{\hat{P}}_z = -\frac{\hat{z}}{(\hat{r}^2 + \hat{z}^2)^{3/2}} - (\hat{F}_{\text{drag}})_z, \quad (18)$$

$$\dot{\hat{P}}_\varphi = -\hat{r}(\hat{F}_{\text{drag}})_\varphi. \quad (19)$$

In equations (14) to (19), the hat sign indicates a dimensionless quantity. We have followed our convention presented in HB03 and have chosen two quantities r_0 and t_0 to represent the units of length and time, respectively, in such a way that $GMt_0^2r_0^{-3} = 1$. The quantities \hat{P}_r , \hat{P}_z , and \hat{P}_φ are the dimensionless radial, vertical and angular momenta of the object, $(r, z) = r_0(\hat{r}, \hat{z})$, $\hat{\mathbf{F}}_{\text{drag}} = t_0^2 \mathbf{F}_{\text{drag}}/r_0$ and $\varphi = \hat{\varphi}$.

4. Numerical Results

To start integrating equations (14) to (19), numerically, we take the mass of the central star to be equal to one solar mass and we choose, $\beta = 1$ and $\rho_0 = 10^{-9} \text{ g cm}^{-3}$. As in HB03, the azimuthal symmetry of the gas density on the midplane of our model nebula allows us to set $r_0 = r_m = 1 \text{ AU}$ which implies $t_0 = 0.16 \text{ years}$.

An important quantity that has to be determined at the beginning of our integrations is the drag coefficient, C_D . As mentioned in the last section, this quantity is a function of the Reynolds number of the gas as given by equation (9). At the beginning of the integration, the initial functional form of C_D is determined by calculating the initial value of Re . During the course of integration, the value of Re is constantly monitored. Once the range of this quantity changes, the integration is continued by adjusting the drag coefficient to its new functional form.

We integrated equations (14) to (19) for different values of solids' radii and densities and also for different values of the gas temperature. The objects were initially placed on circular orbits at different radial positions. The initial height z of an object was taken to be one-tenth of its initial radial distance and $\dot{\varphi}(t = 0) = 0$. The initial velocity along the z -axis was set equal to zero.

4.1. Radial Migration

Figures 2 and 3 show the radial migration of objects with radii ranging from 1 micron to 1 meter. The densities of the objects are equal to 2 g cm^{-3} and the temperature of the gas is 300 K. Each object is once placed at (2,0.2) AU with a radial distance larger than the radial location of the density enhancement on the midplane (i.e., $r = 1 \text{ AU}$), and is once placed at a closer radial distance at (0.25,0.025) AU. As expected, all objects migrate radially in/out toward $r = 1 \text{ AU}$ (HB03). Smaller objects show the tendency of staying with the gas and undergo very slow radial migrations. Larger objects, on the other hand, show more rapid motions. As in the case of the two-dimensional model (HB03), a meter-sized object undergoes the most rapid radial migration.

Figures 2 and 3 also show that the rate of radial migration is greater for inward motions. A result that was also observed in two-dimensional simulations of HB03. This can be attributed to the fact that the rate of change of angular momentum for an object beyond the radial location of the density enhancement is larger than that of an object in a closer distance to the central star. As a result, farther objects lose angular momentum faster, hence, their more rapid radial migration (see HB03 for more detailed analysis).

As mentioned before, as a result of the combined effect of gas drag and pressure gradients, it is expected that objects at radial distances larger than r_m to undergo inward radial migrations. A closer investigation of the results shown in Figures 2 and 3, however, indicates that at the beginning of their radial motions, objects at $r = 2 \text{ AU}$ have, briefly, undergone outward migrations. Figure 4 shows this for a millimeter- and a centimeter-sized particle. Such a behavior can be understood by studying the structure of our model nebula. As given by equation (5), the maxima of the gas density on planes parallel to the midplane at different heights z will appear at different radial distances. Figure 5 shows this for z ranging from zero to 0.2 AU. In the top graph of this figure we have plotted the density of the gas as a function of r for constant values of z . As shown here, the radius of the circular enhancement of the nebula increases from $r = 1 \text{ AU}$ on the midplane to larger values at higher vertical distances. The middle and the bottom graphs of Figure 5 show the gas density enhancement at $z = 0.15$ and 0.2 AU , respectively. When an object is initially at a radial distance beyond

1 AU, depending on its height from the midplane, it may be inside the circle of the local density enhancement at that height. In such cases, the object starts its radial motion by an outward migration while descending toward the midplane. Once it passes the height where the radial distance of the local maximum density is smaller than its instantaneous radial position, the radial motion of the object reverses and it starts its inward migration.

We also numerically integrated equations (14) to (19) for different values of a solid’s density. Figure 6 shows the radial migrations of 1 cm and 1 m solids for different values of their densities. The temperature of the gas is 300 K. Similar to the results of two-dimensional simulations (HB03), increasing the solid’s density results in a more rapid radial migration for a centimeter-sized or smaller particle. However, it has a reverse effect on the motions of meter-sized and larger objects. Such different responses to the change of the density of a solid are the consequences of the contribution of gas drag in changing the rates of its radial migration. Recall that, as mentioned in § 3, the radial component of the velocity of an object relative to the gas is the dominant factor in its radial motion. For a centimeter-sized or smaller object, the magnitude of this component, given by equations (11) and (14), also dominates the magnitude of the relative velocity of the object. Increasing the density of an object while keeping its radius constant results in decreasing the magnitude of the drag force \mathbf{F}_{drag} given by equation (8). Such a decrease in the magnitude of \mathbf{F}_{drag} , in turn, causes the rate of change of the radial component of the relative velocity of the object (equation [17]) to increase, and as a result the object migrates more rapidly.

The situation is not the same for meter-sized and larger objects. In such cases, it is the transverse component of \mathbf{V}_{rel} (equation [13]) that dominates its magnitude. That is, as opposed to small particles, the motion of a meter-sized or larger object is dominated by the rate of the change of its angular momentum. Because the magnitude of \mathbf{F}_{drag} decreases by increasing the solid’s density, from equation (19), a larger value for ρ_p results in a smaller rate for the decrease/increase of the angular momentum of the object. In other words, an increase of the solid’s density will increase its reluctance in losing/gaining angular momentum and hence a decrease in its rate of inward/outward radial migrations.

Numerical integrations were also carried out for different values of the gas temperature. Figure 7 shows radial migrations of a centimeter- and a meter-sized object with a density of 2 g cm^{-3} for four values of the gas temperature. As shown here, increasing the temperature of the gas results in increasing the rate of radial migration. This is an expected result which is the consequence of an increase in the radial component of the pressure gradients of the gas. Figure 8 shows this concept in more detail. In this figure, we have plotted the density of the gas as a function of r on a plane parallel to the midplane at $z = 0.2 \text{ AU}$. As a result of increasing the temperature of the gas from 50 K to 1000 K, the maximum value of the gas

density on this plane is increased by three orders of magnitude. Such an increase implies an increase in the radial component of the pressure gradients of the gas which in turn results in more rapid radial migration.

From equation (5), the radial position of the maximum of the gas density at a certain height z approaches smaller values by increasing the gas temperature. Figure 8 shows this for $z = 0.2$ AU. For an object at this height and at an initial radial position of $r = 2$ AU, such a decrease in the radius of the local density enhancement causes the distance of the initial outward migration of the object to become smaller (Figure 7). For the temperature of 1000 K, the radial location of the maximum gas density at $z = 0.2$ AU becomes smaller than 2 AU and as a result, an object at (2,0.2) AU does not undergo an initial outward migration.

4.2. Vertical Migration

While the combined effect of pressure gradients and the drag force of the gas causes solids to radially migrate toward the location of local density enhancement, the vertical component of the gravitational force of the central star attracts solids toward the midplane of the nebula. Figure 9 shows the vertical motion of solids with different sizes. The dependence of the rate of vertical migration on the size of an object can clearly be seen from this figure. As shown here, except for when the objects are in the vicinity of the midplane, the rates of their vertical migrations increase by increasing their radii. In the vicinity of the midplane, however, while 10 centimeter-sized and smaller objects continue their smooth descent, the 1 meter-sized object undergoes an overshoot. Such an overshoot and its corresponding damped oscillatory motion are more pronounced when the density of the object is increased. Figure 10 shows the vertical migrations of a 1 centimeter-sized and a 1 meter-sized object for different values of their densities. As shown here, the rates of vertical descent of both objects increase by increasing their densities. Once in the vicinity of the midplane, the meter-sized object undergoes a damped oscillatory motion whose amplitude increases by increasing the solid's density. Figure 11 shows the three-dimensional paths of these two objects.

The dynamical behavior of an object along the z -axis and in the vicinity of the midplane can be explained by studying equation (18) in more detail. In this equation, the drag coefficient C_D is the factor that determines the functional form of \dot{P}_z . Substituting for the drag force of the gas from equation (8) and for the z -component of the relative velocity of an object with respect to the gas from equation (12), equation (18) can be written as

$$\dot{\hat{P}}_z = -\frac{\hat{z}}{(\hat{r}^2 + \hat{z}^2)^{3/2}} - \frac{\hat{\rho}_g(\mathbf{R})}{\hat{\rho}_p(\hat{a}_p + \hat{\lambda})} \left[\left(\frac{\hat{\lambda}}{\hat{a}_p} \right) \hat{v}_{\text{th}} + \frac{3}{8} C_D \hat{v}_{\text{rel}} \right] \hat{P}_z. \quad (20)$$

In the following we study equation (20) for $\text{Re} < 1$ and $1 < \text{Re} < 800$. The case of $\text{Re} > 800$ is not studied here since it corresponds to the motions of objects with sizes equal or greater than 100 m. As shown in HB03, the rates of migrations of such objects due to gas drag and pressure gradient decrease by increasing their sizes. In this paper, we focus our study on rapid migration of small solids.

4.2.1. $C_D = 24 \text{Re}^{-1}$

Replacing t_0, K_B, m_0 and σ by their numerical values and considering spherical solids with masses of $(4/3)\pi a_p^3 \rho_p$, equation (20) is written as

$$\dot{\hat{P}}_z \simeq -\frac{\hat{z}}{(\hat{r}^2 + \hat{z}^2)^{3/2}} - \frac{3.73}{a_p(\text{cm}) \rho_p(\text{g cm}^{-3}) [a_p(\text{cm}) + \lambda(\text{cm})]} T^{1/2} \hat{P}_z, \quad (21)$$

where T is in Kelvin. In the vicinity of the midplane, $\hat{z} \ll \hat{r}$ and equation (21) can be simplified to

$$\ddot{\hat{z}} + \frac{3.73}{a_p(\text{cm}) \rho_p(\text{g cm}^{-3}) [a_p(\text{cm}) + \lambda(\text{cm})]} T^{1/2} \dot{\hat{z}} + \frac{\hat{z}}{\hat{r}^3} \simeq 0. \quad (22)$$

Equation (22) resembles the equation of a damped harmonic motion with a dimensionless frequency of

$$\hat{\omega}^2 = \hat{r}^{-3} - 3.48 T \left\{ a_p(\text{cm}) \rho_p(\text{g cm}^{-3}) [a_p(\text{cm}) + \lambda(\text{cm})] \right\}^{-2}. \quad (23)$$

Equation (23) indicates that $\hat{\omega}^2$ is a function of the solid's radius and density, the gas temperature and also the mean free path of the gas molecules, λ . We recall that λ varies with the gas density as mentioned in §3.

At any location in the vicinity of the midplane, the type of the motion of an object depends on the sign of $\hat{\omega}^2$ at that location. The left column of Figure 12 shows the absolute value of the second term of equation (23) for a centimeter-sized object initially at (1.25, 0.125) AU. We chose $a_p = 1$ cm as a representative of solids with $\text{Re} < 1$ since the results of our numerical integrations indicate that the first sign of a Reynolds number larger than unity appears for an object with a radius of 10 cm. Since for an object at (1.25, 0.125) AU, \hat{r}^{-3} varies between 0.512 and 1, the graphs of $\hat{r}^2 - \hat{\omega}^2$, as shown in Figure 12, indicate that

for a centimeter-sized object, $\hat{\omega}^2$ is negative. A negative value for $\hat{\omega}^2$ is an indication of an overdamped motion. Increasing the density of the solid while keeping the gas temperature constant, $\hat{\omega}^2$ becomes larger and approaches zero (critically damped) indicating that the overdamped nature of the vertical motion of the particle weakens and it may even change into an underdamped motion where $\hat{\omega}^2$ is positive.

From equation (23), the overdamping nature of the vertical motion becomes even more pronounced when the radius of the object is smaller than 1 cm. That means, the rate of vertical migration of a solid decreases by decreasing its size (Figure 9).

The left column of Figure 12 also shows that for a constant value of the solid's density, increasing the gas temperature results in lower values for $\hat{\omega}^2$. That means, at higher temperatures, the overdamping of the vertical motion of the object becomes more pronounced (top graph of Figure 13). This can be explained noting that from equation (5) and as shown in Figure 15, at any radial distance r , the vertical distribution of the gas maximizes at $z = 0$ (i.e., on the midplane). As shown in Figure 14, the width of the gas distribution function along the z -axis increases by increasing the gas temperature. As a result of this broadening, the resistive effect of gas drag on the vertical motion of solids appear in a larger range of variable z which results in a longer time for descending toward the midplane.

$$4.2.2. \quad C_D = 24 \text{Re}^{-0.6}$$

In this case, equation (20) can be written as

$$\begin{aligned} \dot{P}_z \simeq & -\frac{\dot{z}}{(\hat{r}^2 + \hat{z}^2)^{3/2}} - \frac{2.44}{a_p(\text{cm}) \rho_p(\text{g cm}^{-3}) [a_p(\text{cm}) + \lambda(\text{cm})]} T^{1/2} \hat{P}_z \\ & \left\{ 1 + 8.56 [a_p(\text{cm})]^{0.4} T^{-0.2} \left[\hat{P}_r^2 + \hat{P}_z^2 + \left(\frac{\dot{P}_\varphi}{\hat{r}} - \sqrt{\frac{1}{\hat{r}} - 9.29 \times 10^{-6} T \hat{r}(\hat{r} - 1)} \right)^2 \right]^{0.2} \right. \\ & \left. \text{Exp} \left\{ 86098 T^{-1} \left[\frac{1}{(\hat{r}^2 + \hat{z}^2)^{1/2}} - \frac{1}{\hat{r}} \right] - 0.4(\hat{r} - 1)^2 \right\} \right\}. \quad (24) \end{aligned}$$

Similar to the previous case, in the vicinity of the midplane, equation (24) can be simplified to

$$\begin{aligned} \ddot{z} + \frac{2.44}{a_p(\text{cm}) \rho_p(\text{g cm}^{-3}) [a_p(\text{cm}) + \lambda(\text{cm})]} T^{1/2} \dot{z} & \left\{ 1 + 8.56 [a_p(\text{cm})]^{0.4} T^{-0.2} \right. \\ & \left. \left[\dot{\hat{r}}^2 + \dot{\hat{z}}^2 + \left(\hat{r} \dot{\hat{\varphi}} - \sqrt{\frac{1}{\hat{r}} - 9.29 \times 10^{-6} T \hat{r}(\hat{r} - 1)} \right)^2 \right]^{0.2} e^{-0.4(\hat{r}-1)^2} \right\} + \frac{\dot{z}}{\hat{r}^3} \simeq 0. \quad (25) \end{aligned}$$

For any value of \hat{r} , equation (25) resembles the equation of motion of a damped oscillator with a dimensionless frequency of

$$\hat{\omega}^2 = \hat{r}^{-3} - 1.49 T \left\{ a_p(\text{cm}) \rho_p(\text{g cm}^{-3}) [a_p(\text{cm}) + \lambda(\text{cm})] \right\}^{-2} \\ \left\{ 1 + 8.56 [a_p(\text{cm})]^{0.4} T^{-0.2} \left[\dot{\hat{r}}^2 + \dot{\hat{z}}^2 + \left(\hat{r} \dot{\hat{\varphi}} - \sqrt{\frac{1}{\hat{r}}} - 9.29 \times 10^{-6} T \hat{r} (\hat{r} - 1) \right)^2 \right]^{0.2} e^{-0.4(\hat{r}-1)^2} \right\}^2. \quad (26)$$

The right column of Figure 12 shows the absolute value of the second term of this equation for different values of the density of a meter-sized object initially at (1.25, 0.125) AU. The radial migration of such an object starts at $\hat{r} = 1.25$ and terminates at $\hat{r} = 1$, implying that the first term of equation (26) will vary between 0.512 and 1. As shown in Figure 12, at a constant temperature and for a given value of \hat{r} , the contribution of the second term of equation (26) is quite small. As a result, the instantaneous dimensionless frequency $\hat{\omega}^2$ stays positive for the entire time of the solid's migration indicating that the motion of such an object, in both sides of the midplane, is an underdamped oscillatory motion.

Figure 12 also shows that the numerical contribution of the second term of equation (26) decreases by increasing the solid's density at a constant temperature. This results in larger frequencies for denser objects which in turn, results in more oscillations (Figure 10). One can also see from Figure 12 that for a constant value of the solid's density, increasing the gas temperature will increase the numerical value of the second term of equation (26). This results in a smaller frequency and less oscillatory behavior (bottom graph of Figure 13). It is necessary to mention that the irregular shape of the second term of equation (26) for $r > 1.25$, is due to the initial outward migration of the solid.

5. Summary and Discussion

We have studied the migration of solids induced by gas drag and pressure gradients in a non-uniform nebula. We considered a rotating, isothermal and turbulence-free gaseous disk with an azimuthally symmetric density enhancement on its midplane and a solar type star at its center. The results of our numerical simulations of the motions of solids ranging from micron-sized particles to meter-sized objects indicated that solids tend to migrate toward the locations of local maximum pressure. In our model nebula, such locations correspond to places where the density of the gas is locally enhanced. Our results indicate that depending on the physical properties of solids, gas drag induced migration can be quite rapid. Such rapid migrations can increase the rates of collision and coalescence of particles and enhance their growth-rates to larger bodies. The results of the extension of this study to include mass-growth and collisional coagulation are currently under preparation for publication.

It is necessary to emphasize that the assumptions of an isothermal and turbulence-free nebula were made merely to focus attention on the sole effect of gas drag on the rate of migration of solids. Also, in this study, we focused our attention on the motion of objects without considering their mutual interactions. In a realistic scenario, one has to allow for the changes of the gas temperature on both radial and vertical directions and also take turbulence and collision into consideration. It is expected that by including turbulence, in particular in the vertical direction, the rate of approach of particles to the midplane of the nebula may decrease. It would then be of utmost value to investigate to what degree the combined effect of turbulence and gas drag induced rapid migration will enhance the rate of the formation of larger bodies. Such studies are currently underway.

This work is partially supported by the NASA Origins of the Solar System Program under Grant NAG5-10547 and by the NASA Astrobiology Institute under Cooperative Agreement NCC2-1056.

REFERENCES

- Adachi, I., Hayashi, C., & Nakazawa, K. 1976, *Prog.Theor.Phys.*, 56, 1756
- Haghighipour, N. & Boss, A. P. 2003, To appear in *ApJ*
- Supulver, K. D., & Lin, D. N. C. 2000, *Icarus*, 146, 525
- Takeuchi, T., & Lin, D. N. C. 2002, *ApJ*, 581, 1344
- Weidenschilling, S. J. 1977, *MNRAS*, 180, 57
- Whipple, F. L. 1964, *Proc. Nat. Acad. Sci.*, 52, 565

Fig. 1.—

See Figure1.gif

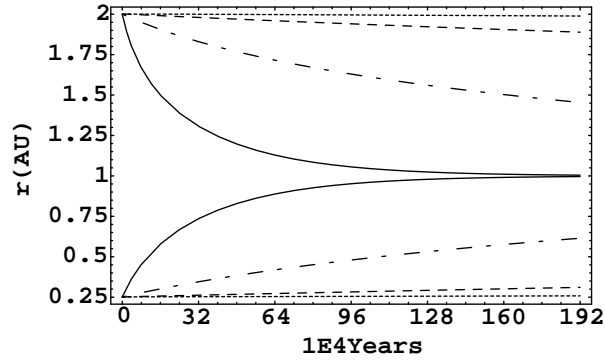


Fig. 2.— Inward and outward radial migrations of small solids from (2,0.2) AU and (0.25, 0.025) AU to (1,0) AU, respectively. The dotted line represents the migration of a micron-sized particle, the dashed line is that of a 10 micron object, the dash-dotted line corresponds to the radial migration of an object with a radius equal to 100 micron and the solid line represents the migration of a millimeter-sized particle. The density of all particles is equal to 2 g/cm³. The physical properties of the gas are similar to those of Figure 1.

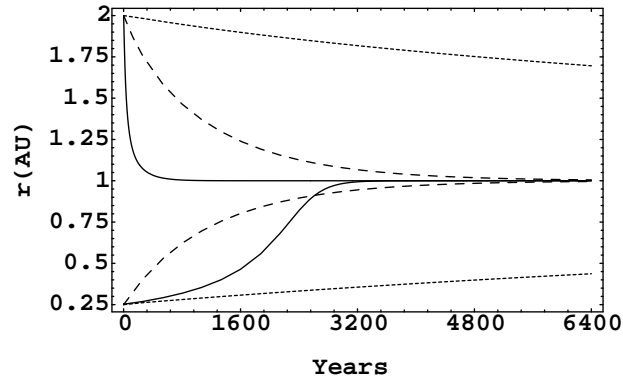


Fig. 3.— Radial migration of centimeter-sized (dotted line), 10 centimeter-sized (dashed line) and meter-sized (solid line) objects. The physical properties of the gas and the solids, and the initial positions of the objects are similar to those of Figure 2. As shown here, meter-sized objects show the most rapid radial migration.

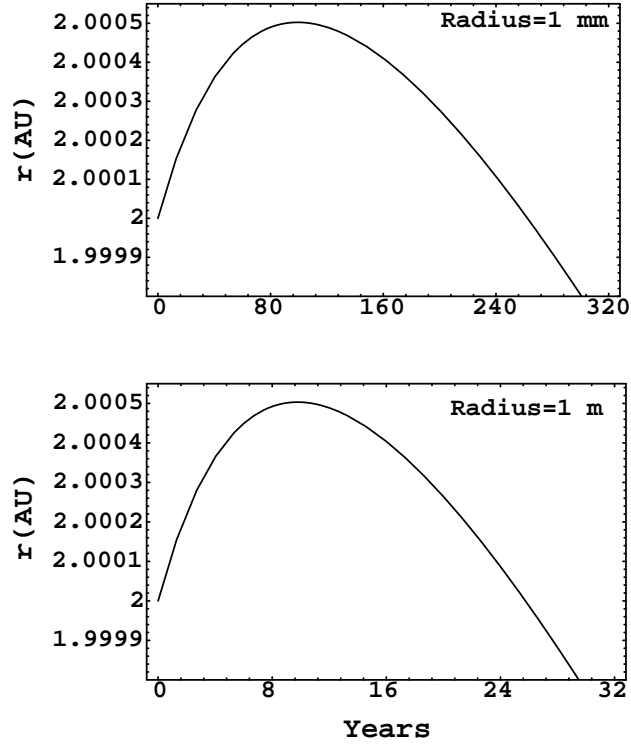


Fig. 4.— Graphs of the initial outward migrations of a millimeter-size particle (top) and a centimeter-sized object (bottom). Objects were initially placed at (2, 0.2) AU. The physical properties of the gas and the solids are similar to those of Figure 2. Note different scales on the time axes.

Fig. 5.—

See Figure5.gif

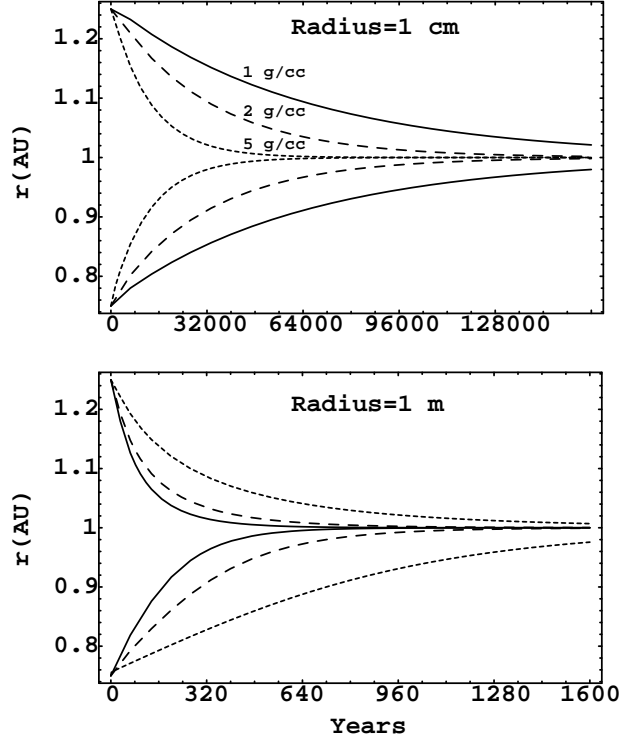


Fig. 6.— Radial migrations of a centimeter-sized particle and a meter-sized solid for different values of the solid’s density. The physical properties of the gas are similar to those of Figure 1. As mentioned in the text, centimeter-sized and smaller particles undergo more rapid radial migrations by increasing their densities. The rate of radial migration of a meter-sized or larger object, on the other hand, decreases by increasing its density. Note different scales on time axes.

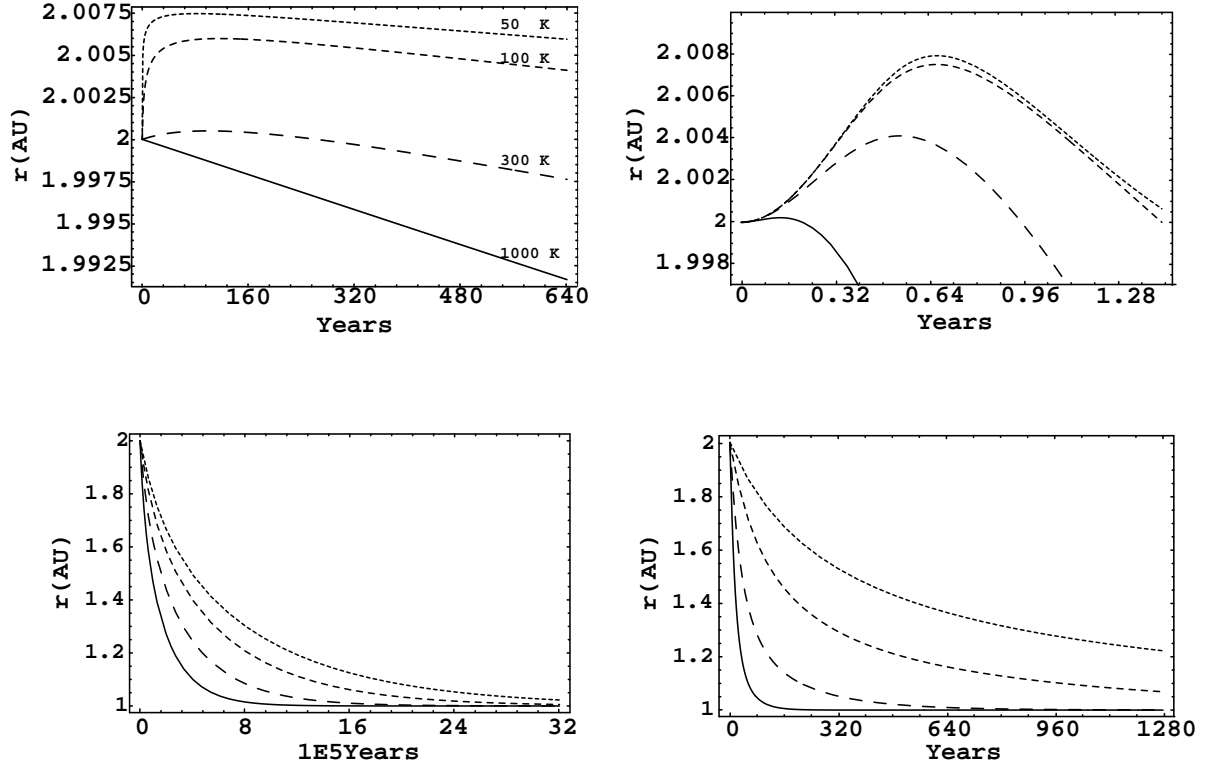


Fig. 7.— Graphs of the radial migration of a millimeter-sized solid (left column) and a meter-sized object (right column) for different values of the gas temperature. The values of ρ_0 , β and r_m are similar to those of Figure 1 and the density of all objects is equal to 2 g cm^{-3} . As seen from this figure, the rate of radial migration increases by increasing the temperature. Note different scales on vertical and horizontal axes.

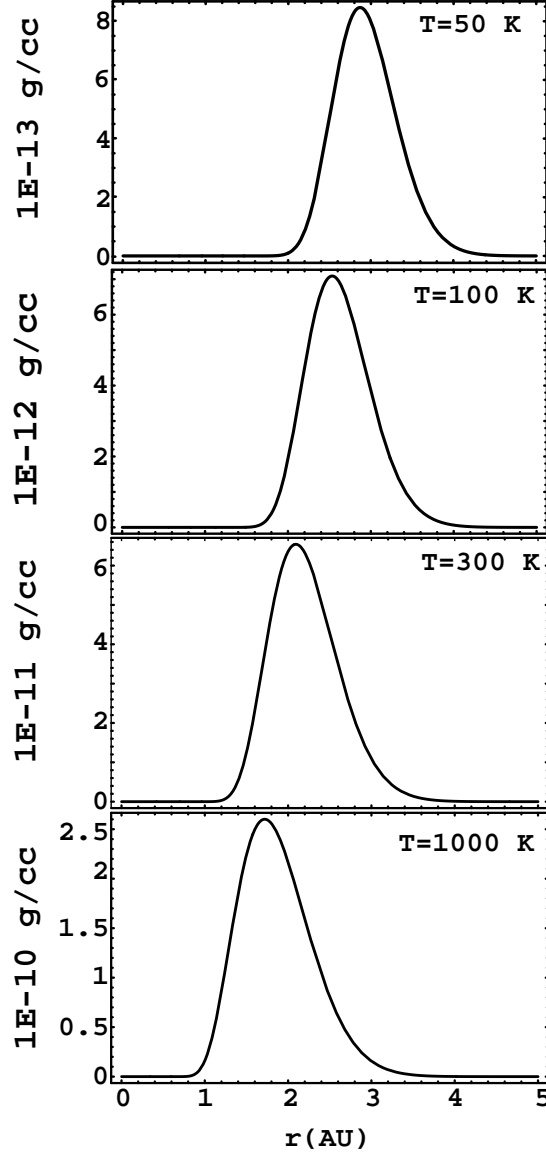


Fig. 8.— Radial distribution of the gas on a plane parallel to the midplane at $z = 0.2$ AU. The values of ρ_0 , β and r_m are similar to those of Figure 1. As shown here, increasing the gas temperature means that the value of the local maximum density increases and its radial location approaches smaller distances. Note different scales on vertical axes.

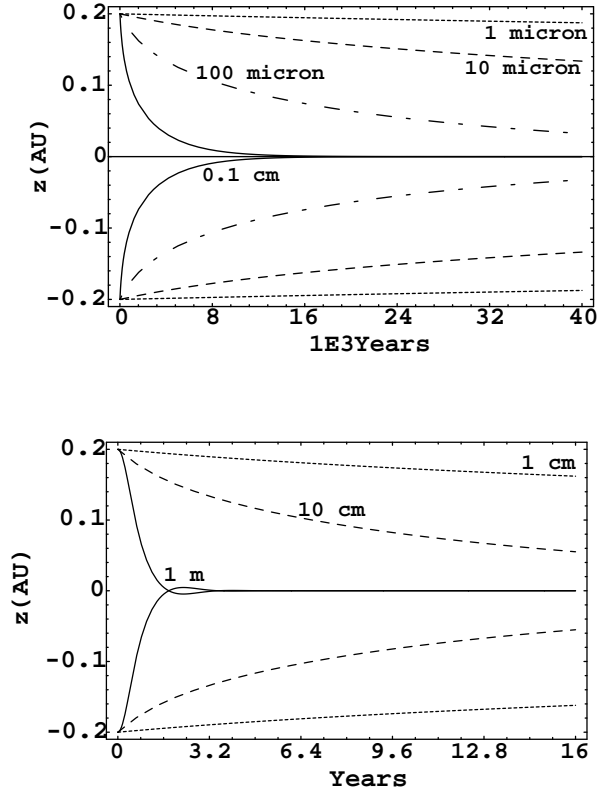


Fig. 9.— Vertical migration of solids. The physical properties of the nebula are identical to those of Figure 1. Each particle was initially at a height equal to one-tenth of its radial distance. Note the different scales on the time axes.

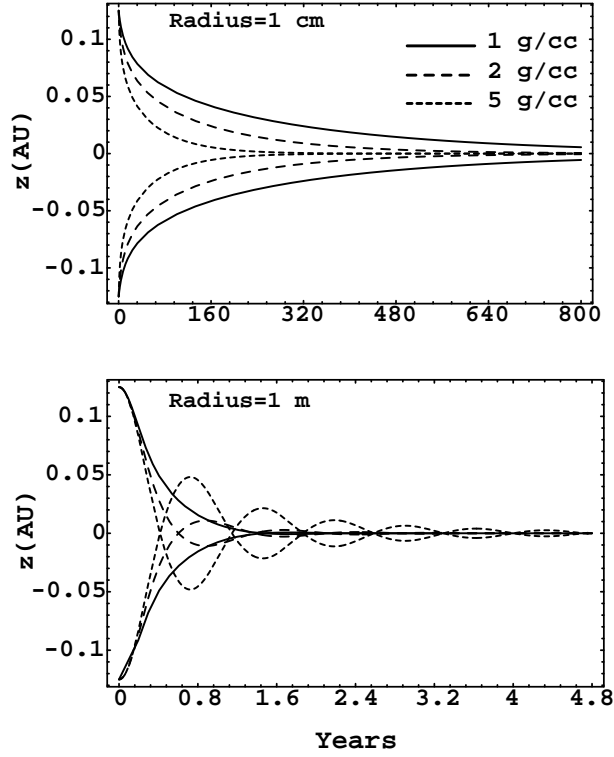


Fig. 10.— Vertical motion of a centimeter-sized particle and a meter-sized object in the vicinity of the midplane, for different values of their densities. The initial positions of each particle is $(1.25, \pm 0.125)$ AU. The physical properties of the nebula are similar to those of Figure 1. As shown here, the motion of a 1 cm solid in the vicinity of the midplane is overdamped while a 1 m object undergoes an underdamped oscillatory motion. The rates of the initial descent of both solids increase by increasing their densities. Note different scales on the time axes.

Fig. 11.—

See **Figure11.gif**

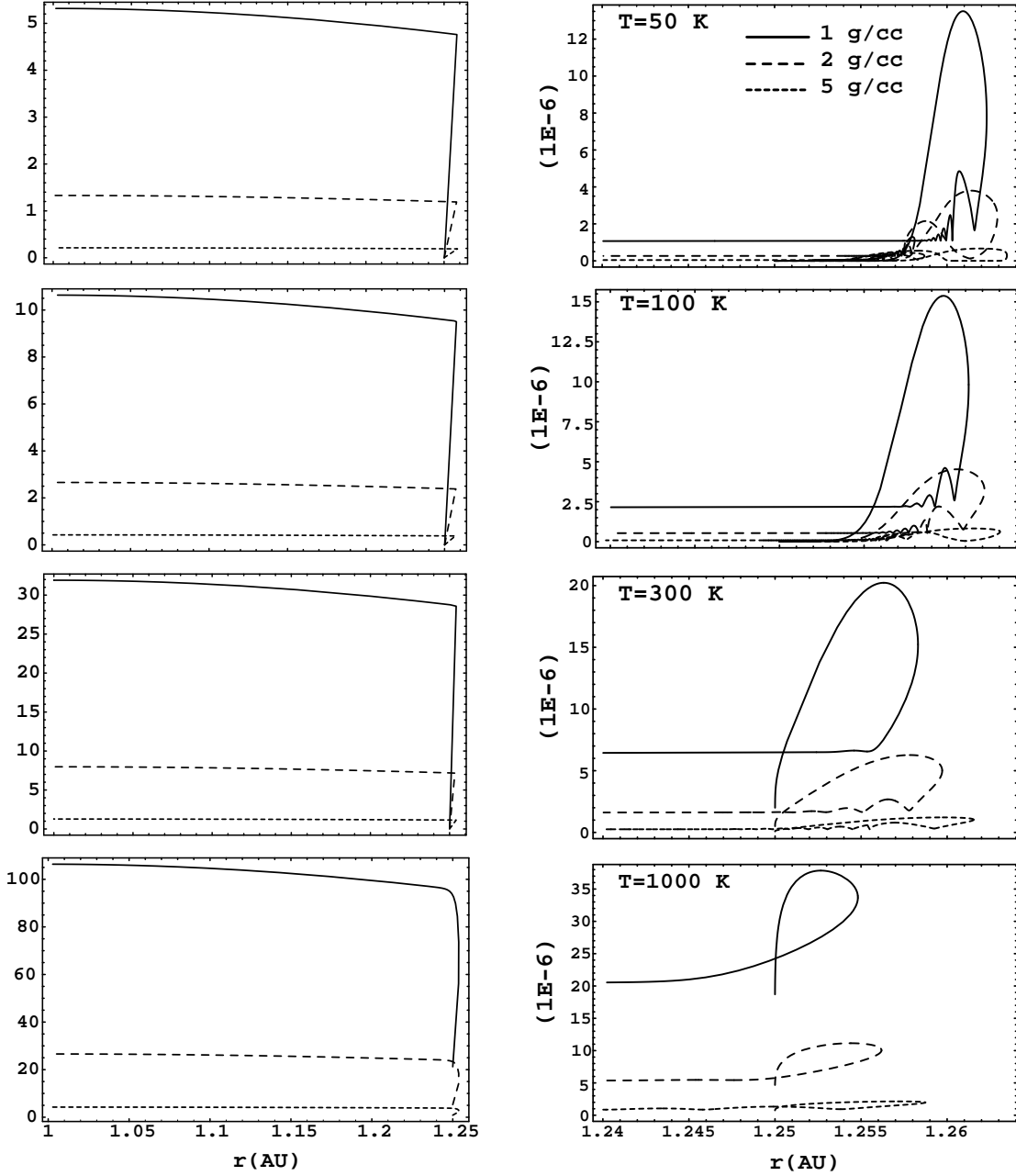


Fig. 12.— Graphs of $\hat{r}^{-3} - \hat{\omega}^2$ versus \hat{r} for a 1 cm particle (left column) and a meter-sized object (right column). The objects were initially at (1.25,0.125) AU. The values of ρ_0 , β and r_m are similar to those of Figure 1.

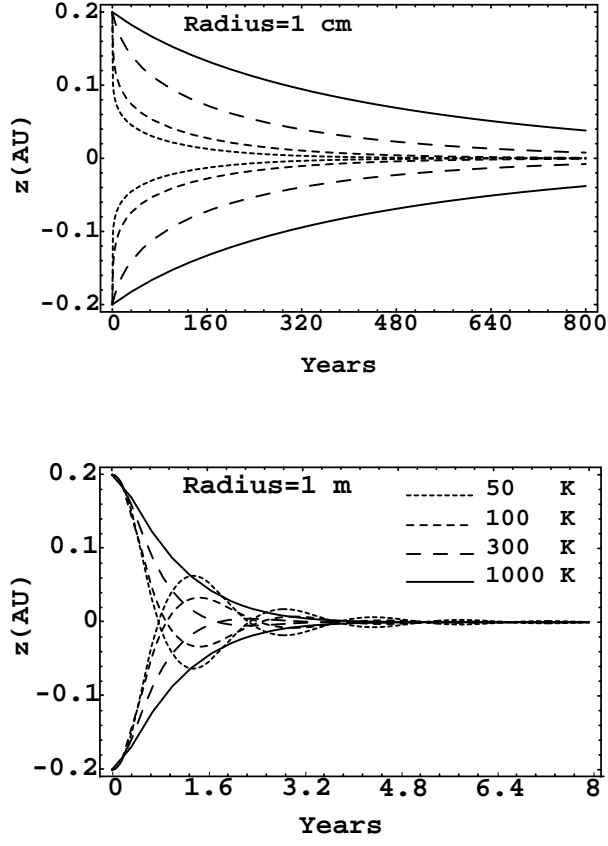


Fig. 13.— Vertical migration of a centimeter-sized particle and a meter-sized object with densities equal to 2 g cm^{-3} for different values of the gas temperature. The values of ρ_0 , β and r_m are similar to those of Figure 1. Both particles were initially at $(2, \pm 0.2)$ AU. Note different scales on time axes.

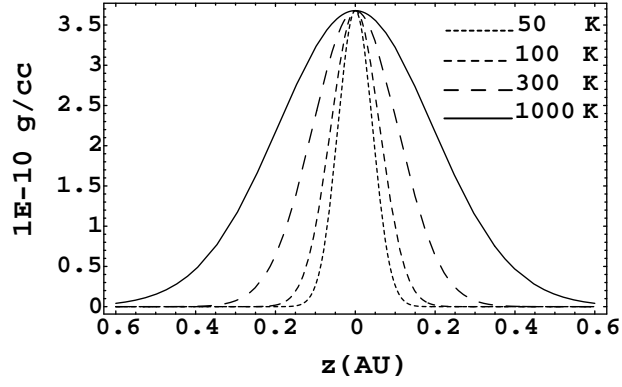


Fig. 14.— Graph of the vertical distribution of gas at $r = 2$ AU for different values of temperature.

Fig. 15.—

See **Figure15.gif**

This figure "Figure1.gif" is available in "gif" format from:

<http://arxiv.org/ps/astro-ph/0305594v1>

This figure "Figure5.gif" is available in "gif" format from:

<http://arxiv.org/ps/astro-ph/0305594v1>

This figure "Figure11.gif" is available in "gif" format from:

<http://arxiv.org/ps/astro-ph/0305594v1>

This figure "Figure15.gif" is available in "gif" format from:

<http://arxiv.org/ps/astro-ph/0305594v1>